Available online at www.sciencedirect.com
SCIENCE DIRECT®
ELSEVIER
Earth and Planetary Science Letters 218 (2004) 215–228
EPSL
www.elsevier.com/locate/epsl

Laboratory measurements of electrical conductivity of hydrous and dry silicic melts under pressure

Fabrice Gaillard *

Bayerisches Geoinstitut, Universität Bayreuth, D-95440 Bayreuth, Germany

Received 7 July 2003; received in revised form 4 September 2003; accepted 31 October 2003

Abstract

An interpretation of the electrical signature of molten rocks within the Earth's interior in terms of nature and temperature conditions of magma requires additional laboratory data on the electrical conductivity of silicate melts. This paper describes an experimental setup and presents measurements of the electrical impedance of dry and hydrous (1–3 wt% H_2O) metaluminous obsidians determined in an internally heated pressure vessel, in the range of 50–400 MPa and 350–1325°C. It is shown that the temperature and pressure dependences of electrical conductivity of both hydrous and dry obsidian can be fitted by an Arrhenius law applying in the melt and the glass regions. This suggests that a similar transport mechanism operates in both melt and glass. The determined activation energies are 70 kJ/mol for the dry obsidian and 65 and 61 kJ/mol for the 1 and 3 wt% H_2O melts, respectively. The activation volume is 20 cm^3/mol. Combination of tracer diffusion and electrical conductivity reveals that sodium is the dominant charge carrier in the hydrous and dry obsidians. The temperature and pressure effects on conductivity are therefore interpreted in terms of activation energy and activation volume for Na mobility in dry and hydrous rhyolites. An increase in conductivity associated with addition of water was observed and is shown to reflect the effect of water incorporation in melts on the mobility of sodium. As a prospective, it is anticipated that both the mobility and content of sodium could control the electrical conductivity of most terrestrial silicate melts. Magma under differentiation becomes more conductive due to sodium and water enrichment associated with fractional crystallization; therefore, its electrical signature must reveal its nature and maturity.

Keywords: electrical conductivity; silicate melt; glass; water; diffusion; Nernst–Einstein equation; pressure; magnetotelluric; volcanic hazards

1. Introduction

Electrical conductivity is a subtle probe of transport properties in silicates, which reveals the mobility and number of charge carriers activated in the presence of a gradient in electrical potential. Therefore, the conductivity of a rock is extremely sensitive to its chemical composition, the nature of its constituting phases and its texture. It is then likely that heterogeneities of conductivity identified from geomagnetic and magnetotelluric data could be interpreted in terms of physicochemical state of rocks within the interior

* Tel.: +49-921-55-37-12; Fax: +49-921-55-37-69.
E-mail address: fabrice.gaillard@uni-bayreuth.de (F. Gaillard).

0012-821X/03/$ – see front matter © 2003 Elsevier B.V. All rights reserved.
doi:10.1016/S0012-821X(03)00639-3

of the Earth [1–6]. Recent reports have brought evidence of highly conductive zones in the crust and upper mantle attributed to the presence of magmas [2,6]. Conducting experiments on partially molten granulites, Roberts and Tyburczy [7] and Partzsch et al. [3] have assessed the effect of melt content on electrical properties of lower crustal rocks, and they proposed that melt fraction and possibly temperature could be evaluated from geoelectrical and magnetotelluric measurements. In these partially molten systems, the conductivity of both solid and liquid contribute to the bulk electrical behavior of the rocks. Glover et al. [8] have articulated a theoretical model predicting how the conductivity, in a two-conducting phase system, evolves as a function of their relative proportion; due to the contrast in conductivity between solid and liquid, the conductivity of the melt is mostly dominant. The spectrum of terrestrial magma compositions is very large and is not covered by the current database of molten silicate electrical conductivity. In particular, melting is often attributable to or at least facilitated by the presence of water. Furthermore, during melting of rocks, water is largely partitioned in the liquid together with alkalis elements. Therefore, most of the magma contains water in the range of ppm to wt% [9], which is likely to severely influence its conductivity. An elucidation of the effect of water on electrical conductivity of silicate melts is subsequently required. Moreover, temperature and, to a lesser extent, pressure affect conductivity. In the absence of reliable laboratory constraints on these physicochemical factors, estimation of melt fraction and nature from electrical conductivity of the Earth's interior might be tentative. This paper presents a system allowing the electrical conductivity of melts to be measured under temperature and pressure in an internally heated pressure vessel. Electrical conductivity measurements are performed on a dry and hydrated natural rhyolite in a P–T range relevant to the terrestrial upper crust. Both temperature and pressure effects on electrical conductivity are determined and the nature of charge carriers in magma is elucidated.

2. Basis of electrical conductivity

As with diffusivity and viscosity properties, the electrical conductivity of silicate melts is a property whose temperature and pressure dependence can be described, in the temperature range of natural magmas, by an Arrhenius law:

$$\sigma = \sigma_0 \exp[(-E_a + P\Delta V)/RT] \quad (1)$$

The expression of conductivity (σ) is here simplified as a function of a pre-exponential term (σ_0)and an activation energy term (E_a), and can also be accounted for by a pressure dependence ($P\Delta V$). For specific silicate melt compositions, it has been shown that the relaxation time and the activation energy of electrical conductivity are similar to that of viscosity [10]. This equivalence is predictable combining the Nernst–Einstein equation, relating electrical conductivity to diffusion properties, and the Eyring equation, which relates diffusion to viscosity. However, Mungall [11] recently evaluated the relationships between diffusion and viscosity data for silicate melts and showed that diffusion rate of network formers matches well with viscosity whereas alkalis, being charge-compensator or modifier cations, show a diffusion behavior decoupled from relaxation times of silicate network (i.e. the Si–O bonds). Therefore, depending on the conduction mechanisms and the nature of charge carriers, electrical conductivity may or may not be predicted from viscosity and vice versa. In natural magmas, several charge carriers are likely to be involved. The total conductivity is the sum of each individual transport mechanisms (1, 2, 3, ...):

$$\sigma = \sigma_1 + \sigma_2 + \sigma_3 + \ldots \quad (2)$$

Although natural magmas are multicomponent and complex systems, their conductivity is generally dominated by one or two transport mechanisms, being much faster than other possible mechanisms. The individual contribution to the bulk conductivity of a charge carrier, i, is defined by the Nernst–Einstein equation:

$$\sigma_i = D_i q_i^2 N_i (kT)^{-1} (H_r)^{-1} \quad (3)$$

D_i is the tracer diffusion coefficient, q_i and N_i are respectively the charge and number of charge

carrier per volume unit, k is the Boltzmann constant and T is the temperature. H_r defines the Haven ratio, which is related to the correlation factor [12]. The Haven ratio of amorphous silicates generally lies between 0.2 and 1, depending on the nature of the diffusion mechanisms [13]. Therefore, combining Eqs. 2 and 3 allows the number and the nature of charge carriers to be determined when σ_i and D_i and their temperature dependences are known.

3. Methodology

3.1. Starting materials

Anhydrous experiments were performed on a natural obsidian that contains 0.1 wt% water (Table 1, [14]). Electrical measurements in the hydrous system were conducted on this obsidian that was pre-hydrated to 1 and 3 wt% H_2O in a pressure vessel (see hereafter). Both dry and hydrated starting glasses are bubble free at the micrometer scale. Their compositions are provided in Table 1. The dry glass was shown to have a glass transition temperature around 800°C at 1 atm [14].

3.2. High-pressure and high-temperature experiments

Experiments were realized in the internally heated pressure vessel of the BGI. The pressure medium was argon and the total pressure was monitored using a Bourdon gauge. A two-Mo-winding vertical furnace was used. Both windings were independently controlled with Eurotherm controllers to reduce the thermal gradient in the sample zone. The thermal gradient was monitored with three thermocouples and reduced to less than 2°C at a pressure below 200 MPa but increased to 10°C over 3 cm at 400 MPa. However, combining all runs, the average thermal gradient within the 3 cm where the thermocouples were placed was 3°C. The temperature of the 3.5 mm sample was monitored with a thermocouple placed next to it. The hydration of the obsidian was performed at 1150°C and 200 MPa during 3 days for the 3 wt% H_2O sample and at 1250°C, 200 MPa for 4 days for the 1 wt% H_2O sample. Powders of the glass were loaded and welded in a Pt capsule (8 mm diameter, 3 cm length) together with the wanted amount of distilled water. After synthesis, hydrous glasses were inspected to check for the presence of bubbles and all of them where clear glasses. Electron microprobe analyses were conducted to check for chemical changes and water content was determined by infrared spectroscopy following the procedure described in [14].

Redox conditions in the pressure vessel were not determined. We estimated that oxygen fugacity in dry melt was around the nickel–nickel oxide buffer and the hydrous sample was slightly more oxidized ($\sim$NNO+1). Given that no buffer was used and no H_2 was loaded in the pressure vessel, reduction by H_2 associated with hydration of the melt is not expected [14,15]. To verify this hypothesis, infrared spectra were collected on the dry sample after experiments and no hydrogen enrichment were observed compared to the starting products. Therefore no changes in the sample redox state were likely (see [14], for the relationships

Table 1
Composition of the starting 'dry' obsidian (see [14])

SiO_2	TiO_2	Al_2O_3	MgO	FeO	CaO	Na_2O	K_2O	OH[a]	Fe^{3+}/Fe^{tot} [b]
74.51	0.10	13.25	0.08	1.60	0.75	4.15	5.64	0.125	0.2
0.55	0.06	0.12	0.05	0.08	0.04	0.06	0.10	0.004	0.05

The hydrated obsidians contain 1.05 and 3.1 wt% H_2O but their compositions in terms of major elements were the same as the starting dry obsidian.
Numbers are wt% values, except Fe^{3+}/Fe^{tot} expressed in atoms. The first row is composition and the second one is standard deviation or uncertainty for the ferric–ferrous ratio.
[a] Obtained by FTIR. No molecular H_2O was detected.
[b] Obtained by Mossbauer spectroscopy.

between H and redox exchanges). Another source of redox modification is iron loss in the metal capsule (see Section 3.3 for details of the capsule assemblage). This point is treated in the following but alteration of redox conditions by this way is also excluded.

The sample holder was used to suspend the sample in the pressure vessel and to supply two wires (electrodes) for the conductivity measurements (Fig. 1).

3.3. Conductivity cell and conductivity calculation

The sample geometry and the cell design are given in Fig. 1. In most hydrothermal and gas pressure experiments, the sample is, in general, enclosed in a welded noble metal capsule. In our case, noble metals, being good electrical conductors even at high temperature, exclude the use of a closed capsule. Previous workers mainly performed electrical conductivity measurements in piston cylinder apparatus with two electrodes symmetrically abutted to the molten sample enclosed in a solid container such as SiO_2 glass or MgO [16]. In such a setup, the capsule is not sealed and so, in a gas pressure vessel, argon is likely to incorporate the sample, which may affect the conductivity. Also, water that has to be maintained in the sample during the measurements at P and T may escape if the electrical cell is not sealed in an impermeable membrane. Furthermore, depending on its geometry, the cell might undergo distortions, modifying the electrode–electrode distance. As it is critical to accurately know this distance, a system undergoing the minimum of deformation has to be used. Instead of adopting mirror symmetry for the electrode–sample–electrode system enclosed in a solid container, we adopted a radial electrode–sample–electrode symmetry with the capsule being used as the outer

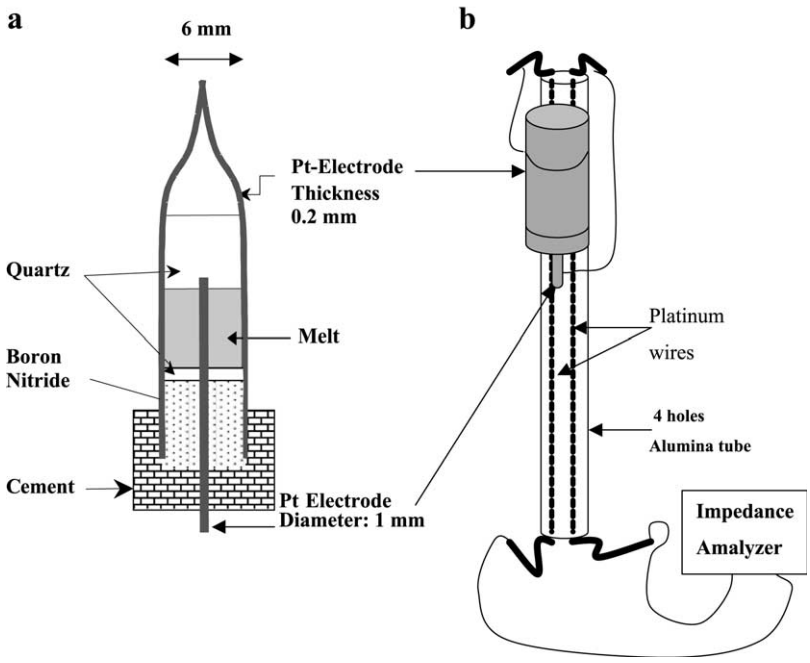

Fig. 1. Experimental setup and design of the conductivity cell. (a) A sketch of the electrical cell. The capsule is 2 cm long and ~2.3 cm with the boron nitride cone and cement lid. The melt (2–4 mm long) is sandwiched between two quartz slices, which avoid any deformations. The inner and outer electrodes are connected to thick Pt wires (∅: 1 mm, panel b) that are connected outside of the vessel to the impedance analyzer. The course of the electrodes from the impedance analyzer to the cell includes several materials (Alumina, cement, BN, quartz), but the obsidian is by far the most-conducting path and therefore the impedance of other materials can be neglected.

electrode (Fig. 1). The capsule is made of platinum (outer ∅: 6 mm) with a wall thickness of 0.2 mm. The inner electrode is a platinum wire (∅: 1 mm). Cylinders 3.5 mm long and of 5 mm ∅ were respectively cored from the starting hydrous and dry glass and an inner hole of 1 mm ∅ was drilled in the center of each sample for the inner electrode. One end of the capsule was arc-welded, whereas, the other end was closed using a BN cone through which the inner electrode passed. To ensure the sealing of the assembly with respect to argon and water, SiO_2–PO_3–H_2O-based cement with a low thermal expansion was used. In order to ensure the stability of the cell geometry, a thick platinum capsule was used and the glass cylinder was sandwiched between two slices of quartz (Fig. 1). After each experiment, the cell shape was checked and no significant deformation was detected. The extent of chemical interactions between quartz and the melt phase was checked by systematic EMPA profiles and was shown to be negligible even after a 3-day experiment at 1250°C. The extent of SiO_2 dissolution in the melt and its effect on the measured impedance are therefore neglected. Another source of change in the cell geometry is the thermal expansion. For platinum, we calculate that thermal expansion from 25 to 1300°C should induce a change in the cell geometry of less than 1%. We therefore neglected it. For the melt, changing temperature from 25 to 1300°C should increase its volume by 6% (using the volume data of Lange and Carmichael [17]). The design of the cell (Fig. 1) allows a vertical expansion through the inner hole of the quartz wafer. Therefore, the expansion of the melt occurs vertically and does not damage the cell geometry. By performing blank experiments (without obsidian in the cell) it was shown that the contribution of quartz, the BN, the cement and the alumina tube to the impedance measured is negligible. The measured impedance, which was probably the BN contribution, was higher than the impedance of the obsidian at a given temperature by a factor of 10^3–10^4. Therefore, the obsidian sample was the only conductive path.

Differential thermal expansion of the different materials used was in part responsible for some dehydration of the sample during measurements at high temperature. Although the run on the hydrous samples was short (< 12 h), evidence of dehydration were brought through infrared analyses (FTIR) on the quenched glass. The water content and distribution in the glass were determined using a Bruker IFS 120 HR high-resolution FTIR spectrometer (see [14] for additional details). Fig. 2 reveals that total water concentration in the 3 wt% H_2O sample dropped from 3 to 1.5 wt% at the quartz–melt interface on the boron nitride side (not-welded side). The other side of the sample had undergone only a partial dehydration from 3 to 2.5 wt%. No radial gradient were found. In all, it appears that 80 volume % of the sample contain between 2.5 and 3 wt% water at the end of the run. Most of this dehydration must have occurred in the last minutes of the run, when high-temperature conditions were reached (> 1300°C). Using data for diffusion of water in melts given in [18], the profile shown in Fig. 2 would correspond to an exposure of 20 min at 1300°C of a similar melt to a dry atmosphere. At lower temperature, it is calculated that a lower diffusion rate of water limited the extent of dehydration. The 1 wt% H_2O sample showed absolutely no evidence of dehydration. FTIR profiles on this sample reveal the absence of any gradient in water content. The reason for this is probably the combination of the relatively low water content (the water diffusion rate increases with in-

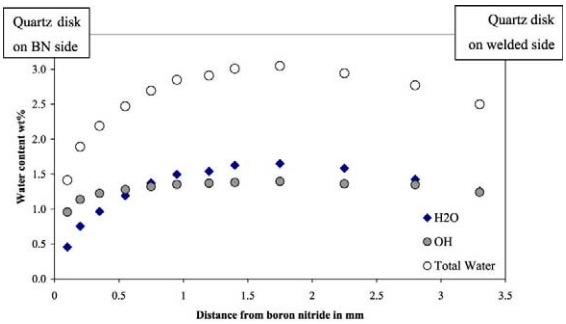

Fig. 2. FTIR profiles of water-derived species in the pre-hydrated sample after measurements at *P* and *T*. Dehydration occurs toward the left where the BN cone and the cement are, but note that > 80% of the sample contains between 2.5 and 3 wt% water. The shapes of the profiles are due to the fact dehydration occurs essentially through migration of molecular H_2O [22].

creasing water content [18]) and the fact that measurements were performed at $T < 1200$°C, a relatively low temperature compared to the run with 3 wt% H_2O.

The conductivity (Ω^{-1} m^{-1}) is calculated from resistance measured with the impedance analyzer using the following equation [19]:

$$\sigma = (R)^{-1}[2\pi l(\ln(r_o/r_i))^{-1}]^{-1} \quad (4)$$

R is the resistance, and l, r_o and r_i are respectively the length, outer radius and inner radius of the sample (see Fig. 1b). As changes in the cell geometry parameters, l, r_o and r_i, were small, uncertainty in conductivity calculation was dominated by uncertainty in R, measured with the impedance analyzer. Incorporations of iron in the outer (capsule) and in the inner (wire) electrode are likely to occur and could potentially affect the measurements of the sample resistance or at least the melt-electrode interface resistance. Electron microprobe analyses were conducted on quenched sample–capsule assemblages after 3 days at 1250°C. No iron was detected in platinum and the Fe content of the glass was shown to be homogeneous and similar to that of the starting material. Alteration of the impedance measurements by iron diffusion into the electrodes is therefore excluded. Eventually, uncertainty in the measured resistance was estimated from repeated measurements at the same P–T conditions as a function of time. In addition, P–T cycles were performed to check if some irreversible damage of the cell could occur. In all case, repeated measurements agreed fairly well, for given P, T conditions, the measured variations of resistance were less than 3%. Only the 3 wt% H_2O experiment has shown an alteration probably due to dehydration at high temperature. The resistance measured at 1050°C after the high-temperature stage was 41.5 Ω against 38.5 Ω before the high-temperature treatment. The two points are discussed in the results part. This increase in resistance of 8% was attributed to a partial release of water (Fig. 2). In spite of this, no corrections were applied to the resistance values. The high-temperature data on the hydrous melt may slightly underestimate (max 8%) the real conductivity of a 3wt% water-bearing obsidian.

3.4. Impedance spectra and resistance of the sample

Silicate solids or liquids display electrical impedance that is a function of the electrical frequency. Therefore, an apparatus producing an alternating current over a large frequency domain was used. A Solartron 1260 impedance gain phase analyzer with a 100 mV applied voltage was used [5]. Most data were obtained in the frequency range of 1 kHz–2 MHz. The electrical response of the sample in this frequency range is equivalent to that of a resistor in series with a resistor and a capacitor in parallel [20]. Therefore, from impedance spectroscopy, one can extract a conductivity value and also an electrical relaxation time (see the caption of Fig. 3). At high temperature (> 1000°C), the measured resistance was lower than 100 Ω and only at frequencies higher than 10^4 Hz, the measured impedance was dominated by the sample. Below this frequency, the impedance spectrum was dominated by the sample–electrode interface impedance (Fig. 3, see also

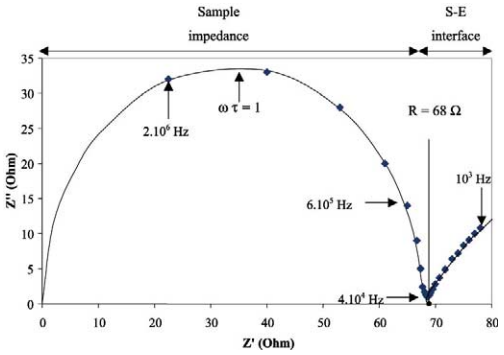

Fig. 3. Impedance spectrum showing a complex plane plot of the imaginary part Z'' vs. real part Z' of the electric modulus for the dry rhyolite at 1100°C, 400 MPa. Frequency values are indicated in Hz for selected data. Basically, frequency decreases from left to right in the diagram. The circle results from a fit of the data in the frequency range of 2×10^6–4×10^4 Hz. At the circle top, $\omega\tau = 1$ means that the frequency of the applied sinusoidal voltage equals the frequency of electrical relaxation of the rhyolite [39] (this frequency should be close to the frequency of Na jumps in the melt, see Section 5). For this spectrum, we calculate a relaxation time of $\sim 10^{-6}$ s. For a frequency lower than 4×10^4 Hz, the sample–electrode (S–E) interface impedance dominates the signal. The frequency dependence of this interface impedance is fitted using a CPE as described in [20].

[20]). The sample resistance R (i.e. ohmic resistance) is derived from the low-frequency intersection of the impedance semicircle with the X-axis. The value for R is directly readable in Fig. 3 as $\sim$68 Ω. Applying a circle fit gives a value for R that is twice the radius of the impedance circle plus a resistance, r, accounting for the fact that the circle does not systematically start at 0 [20]. When possible, this fitting method was used to extract a value for the sample resistance. The electrical relaxation time corresponds to the frequency at which the imaginary component (Z'') of impedance is greatest (top of the circle in Fig. 3). In the frequency region $\sim$MHz, where the electrical response of the sample occurs, the high-frequency part of the spectra were affected by electrical noises probably related to the inductance of the wires connecting the impedance analyzer to the sample [20]. The electrical noise of the furnace is not thought to affect the measurements since it has a frequency of 50 Hz, therefore far below the frequency explored for conductivity measurements. In addition, several tests were performed by switching off and on the furnaces during conductivity measurements and no alterations of the impedance spectra were observed. These statements suggest that the electrical noise of the furnace is not responsible for the high-frequency perturbation of the signal and, rather, the wires connecting the impedance analyzer to the sample must cause most of the high-frequency noise. In fact, Fig. 3 shows one of the rare spectra for which the high-frequency part was properly measured. For $\sim$80% of the spectra, only the frequency part where the circle crosses the X-axis and the sample–electrode interface was accessible. In that case, fitting a semicircle was not feasible, and R_{sample} was calculated by fitting the sample–electrode interface with a constant-phase element circuit (CPE) described in [20], taking into account the R_{sample} value. When both high- and low-frequency regions were properly collected, crosschecking of both methods of R calculation (fit of the circle or fit of the sample–electrode impedance) yielded results in agreement within 2%. Due to this lack of complete information at high frequency, a systematic investigation of the electrical relaxation as a function of temperature and pressure was precluded, and in the following, we focus on the ohmic (DC) conductivity results.

3.5. *Equilibrium achievement at* P *and* T

Dry experiments were started at 1300°C whereas hydrous runs were started at 1050°C (1 wt%) and 950°C (3 wt%) in order to anneal the melt and to optimize the wetting of the melt on the electrodes. During this process the conductivity was measured in order to monitor the time required to achieve a steady state regime. The results are shown in Fig. 4, where the resistance is plotted as a function of time. Within 15 min a steady value is attained at 1300°C for the dry sample. For the hydrous run, $\sim$35 min were required to achieve a steady value. To investigate the effect of temperature and pressure, the set point of the Eurotherm regulator was changed to the desired value, pressure was then readjusted and successive measurements were performed until a stable resistance was observed. Within less than 15 min at the set P and T, a constant value of resistance was measured. At temperature below $\sim$950°C for the dry melt and $\sim$900–850°C for the hydrous one, crystallization should occur in response to a greater thermodynamic stability of minerals vs. melt. Probably due to the high viscosity of this rhyolite at such temperatures, no evidence of crystallization was found after experiments. Similarly, conducting experiments for several days on the same rhyolites at different temperatures, no changes in the crystal content were observed [14]. Therefore, the sample is thermodynamically un-equilibrated, but the slow re-equili-

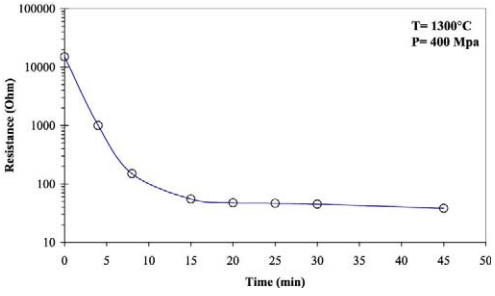

Fig. 4. Evidence of achievement of steady resistance within the first minute of an experiment at 1300°C.

bration rate allows steady measurements to be performed.

The results we present in the following part are results of a dry experiment that has been duplicated to check for consistency. Hydrous runs were not duplicated. In all, dry experiments lasted 2–3 days whereas the hydrous runs lasted 10–15 h.

4. Results

Conductivity of the dry rhyolitic melt is shown in Fig. 5 as a function of temperature variations in the range of 800–1300°C. In this temperature range, the isobaric conductivity is described by an Arrhenius law. The pressure dependence of the conductivity can also be accounted for by the Arrhenius law as indicates Eq. 1. The values fitted for each constant of Eq. 1 against the set of data points shown in Fig. 5 are available in this figure. In Fig. 6, conductivity results over a large temperature range (1300–350°C) are shown. No break in the Arrhenius line was detected at the glass transition temperature, which was estimated for this glass in a previous study at ~800–850°C [14].

Conductivity of the hydrous rhyolites at 200 MPa is shown in Fig. 7 as a function of temperature. For both composition, data are described by an Arrhenius law in the temperature range of 1325–500°C. As the water content increases from 1 to 3 wt%, the conductivity increases slightly. For comparison, the conductivity of the dry rhyolite calculated at 200 MPa using Eq. 2 and the parameters in Fig. 5 is also shown. At low temperature, the conductivity of the 3 wt% H_2O rhyolite is 0.5 log unit higher than the conductivity of the dry sample. With increasing temperature, the difference decreases.

At $T = 1050$°C, for the 3 wt% H_2O sample, two data points are shown. The difference between the two conductivity values corresponds probably to the dehydration effect at high T. One conductivity data was collected during the heating step while the second conductivity value was obtained after the high T stage (to 1325°C). The difference between the two values allows an estimation of the minor effect of partial dehydration on the electrical conductivity of the hydrous obsidian.

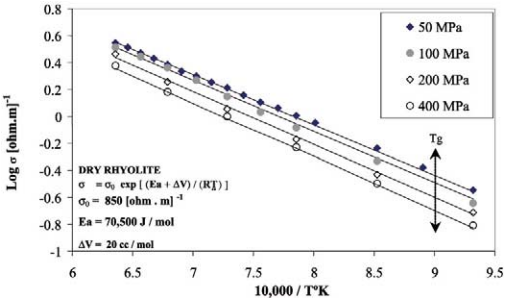

Fig. 5. Arrhenius plot of the conductivity results for the dry obsidian in the temperature range of 1300–800°C. Both temperature and pressure effects can be reproduced using an Arrhenius law whose parameters are shown in the figure. The error bars are smaller than the size of the points. T_g refers to the glass transition temperature.

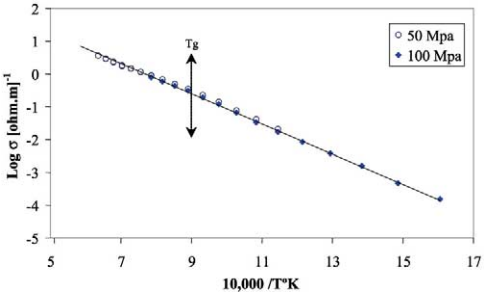

Fig. 6. Arrhenius plot of the conductivity results in the temperature range of 1300–350°C. The temperature effect can be reproduced using a single Arrhenius law for both the melt and the glass region. The error bars are smaller than the size of the points.

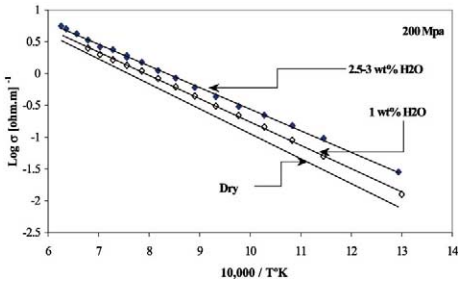

Fig. 7. Arrhenius plot of the conductivity results for hydrous obsidians in the temperature range of 1325–500°C at 200 MPa. The temperature effect can be reproduced using an Arrhenius law whose parameters are shown in the figure. For comparison, the conductivity of a dry obsidian at 200 MPa calculated using the parameters in Fig. 5 is shown. The error bars are smaller than the size of the points.

5. Interpretation

5.1. Charge carriers in dry and hydrous obsidian

The electrical conductivity of both dry and hydrous obsidians is reproducible using an Arrhenius fit. It is therefore likely that a single transport mechanism dominates the electrical conductivity in the melt and glass regions of these obsidians. The most mobile species in these melts are lithium and sodium [13,21,22]. Proton migration is precluded since it is known to move as neutral molecular H_2O or H_2 in obsidian glass and melt [14,23] – species that obviously do not participate in charge transport. Nevertheless, recent conductivity data on hydrated $BaSi_2O_5$ glasses reveal that protons may potentially act as charge carriers in glass with a low degree of polymerization [24]. In contrast, the obsidian composition investigated in this study is fully polymerized; moreover, extrapolations of proton conductivity [24] to temperature of this study fall far below the conductivity values that were measured in the obsidian. It is therefore anticipated that protons do not significantly contribute to the charge transfer in obsidian. According to Jambon [21], both alkalis (Li, Na) have the same mobility in an obsidian melt at a given temperature; however, the low Li content (<500 ppm) should make its contribution to the bulk conductivity negligible. Electronic conductivity could also occur due to the presence of iron in both ferrous and ferric forms. However, to our knowledge, evidence of electronic conduction in natural silicate melts is not reported in the literature. Only iron-rich glasses at low temperature were shown to behave as electronic conductors [25,26]. For our sample, its low iron content together with the high-temperature conditions precludes any significant electronic conduction. Using Eq. 3 and postulating that sodium is the dominating charge carrier, we calculated its diffusion coefficient from conductivity data on the dry obsidian, assuming that all available Na is involved in the transport process. A Haven equal to 1 was adopted. The results of this calculation are shown in Fig. 8, where D_{Na} calculated from conductivity data on the dry sample is plotted against temperature together with the Na tracer diffusion coefficient measured in [21] in dry obsidian melt. The perfect agreement between calculated and measured values clearly reveals that Na is the dominating charge carrier in dry obsidian. Other ionic/electronic contributions can be neglected given that their mobility is at least one to several orders of magnitude slower than that of Na.

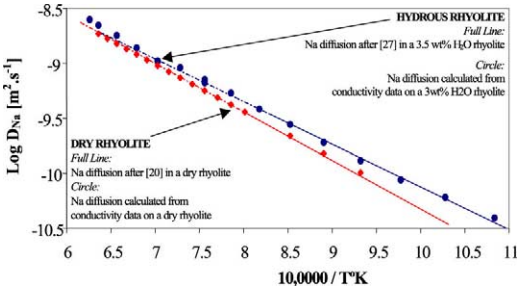

Fig. 8. Identification of Na as the dominating charge carrier in the dry and the hydrous rhyolites. The tracer diffusion coefficient of Na in dry obsidian [21] is plotted together with the diffusion coefficient calculated from the conductivity data at 300 MPa. At a temperature higher than 1000°C, the tracer diffusion data of [21] data are extrapolated (dashed line). The tracer diffusion coefficient of Na in a rhyolite containing 3.5 wt% water (determined in the temperature range of 700–900°C [28]) is plotted together with the diffusion coefficient calculated from the conductivity data of the hydrated obsidian at 200 MPa. Above 900°C, extrapolation of the diffusion models [21–28] deviates from our prediction. We therefore improve the diffusion data on Na in the high-temperature domain. At 1050°C for the hydrous system, two data are shown. The highest D_{Na} is before the high-temperature step and the lowest is after. This gives an idea of the effect on the measurements of dehydration subsequent to the high-temperature treatment.

The activation volume we extracted from the fit in Fig. 5 should therefore reveal the pressure effect on Na mobility in dry silicic melts. The value we obtained from the Arrhenius fit (20 cm^3/mol) indicates a large effect of pressure at least in the crustal pressure domain. Relating this pressure effect to the size of the charge carrier is probably tentative. However, such an activation volume is in good agreement with the pressure dependence of conductivity of Na–borosilicate or Na-bearing organic glasses recently resolved by material scientists [27]. This pressure dependence seems, therefore, to be a feature of Na-rich glasses–melts whose conductivity is dominated by Na migra-

tion. Also, Tyburczy and Waff [16] found a similar activation volume for the conductivity of a Na-rich andesite ($\sim$18 cm^3/mol).

For the hydrous obsidians, their conductivity is slightly higher whereas its activation energy is slightly lower than that of the dry obsidian (Fig. 7). These observations are consistent with the effect of water on the mobility of sodium identified by Watson [28] for obsidian containing 3.5 wt% water. In Fig. 8, tracer diffusion of Na calculated from conductivity data on the 3 wt% H_2O obsidian is plotted against temperature together with tracer diffusion of Na measured by Watson [28] on a similar composition. In the temperature range of 700–900°C, corresponding to the domain covered by [28], the agreements between predicted and measured diffusion coefficients are good, suggesting that sodium controls the conductivity of the most hydrous rhyolite studied. Consequently, the conductivity of the 1 wt% H_2O obsidian must also be controlled by Na mobility. At higher temperature, extrapolation of Watson's model deviates from our prediction. This deviation is probably explained by the propagation of the uncertainty in activation energy given by Watson at high temperature.

Two attempts to measure the electrical conductivity of dry and hydrous silicate melts are available in the literature. Lebedev and Khiratov [29] performed measurements in a pressure vessel using unspecified cell geometry. The frequency of the AC measurements was 100 Hz, a frequency at which this study clearly shows that the sample–electrode interface dominates the measured impedance (Fig. 3). The activation energy for electrical conductivity they estimated also decreases as the melt water content increases. However, the conductivity values they obtained differ by a factor of 10–100 from the results of this study. Given the lack of technical details given in [29], it is difficult to determine the exact nature of this divergence. Shatherley and Smedley [30] performed similar measurements on dry and hydrous (4 wt% H_2O) alkali-rich melts in the frequency range of 1–20 kHz. At the highest-pressure conditions of their study (135 MPa), the effect of water they determined is almost consistent with this study (at least at $T<900$°C). However, their low-pressure experiments, which are strongly water oversaturated, seem to indicate a strong dehydration of the melt in either the form of water-bearing bubble within the melt or an insulating layer of vapor at the sample–electrode interface (vapor being insulator in comparison to the silicate melt). The extent of this dehydration, which is kinetically enhanced by high temperature, is most likely responsible for the decrease in conductivity they observed as the temperature increases.

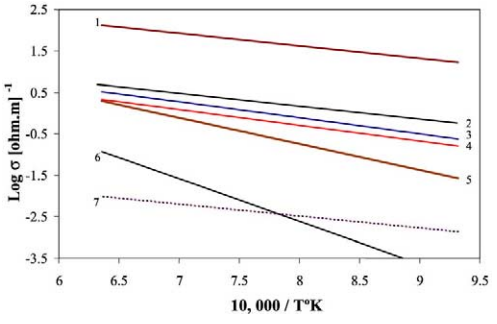

Fig. 9. Temperature dependence of ionic conductivity in dry Na_2SiO_3 liquid (1), 3 wt% H_2O rhyolite (2), dry rholite (3), andesite (4), Na-bearing basalt (5), Na-free basalt (6), and extrapolation toward high temperature of electronic conductivity in Fe-rich glasses (7); references [13,16,25,3,33] and see Section 5.3.

Combining the above elements of discussion and the fact that the Nernst–Einstein equation was successfully applied to our measurements, it appears that this study provides robust data on the electrical conductivity of hydrous silicate melts, which should be considered for the interpretation of partially molten region observed by the magnetotelluric survey. This study allows the individual effect of water, temperature and pressure on the conductivity of silicic melts to be predicted. In Eq. 1, the dependence of the pre-exponential and the activation terms to the water content was accounted for by an empirical fit. The electrical conductivity of hydrous rhyolitic–granitic melts should be calculated as follow:

$$\sigma_{(\Omega\,\mathrm{m})^{-1}} = \sigma_0 \exp[(-E_a + 2P)/RT] \quad (5)$$

with

$$\sigma_0 = -78.9 \ln[\mathrm{wt\%\ H_2O}] + 754$$

$$E_a = -2925 \ln[\text{wt\% } H_2O] + 64132$$

where wt% H_2O is the total water content of the melt expressed as H_2O wt%. Extrapolation of these equations to 6 wt% of water content should remain reasonable. At higher water content, it is likely that water, by dilution, would decrease the Na concentration and then decrease the electrical conductivity of the melt.

5.2. Transport properties in silicic melt

No change in the current transport mechanisms is observed at the glass transition temperature (T_g). The Arrhenius formalism is applicable in the entire temperature range investigated in this study. Therefore, the glass transition temperature or the closure temperature associated with electrical relaxation is very low and could be far below 350°C, the minimum temperature investigated in this study (Fig. 6).

The strongly linear temperature dependence of electrical conductivity reminds us of the viscous properties of 'strong' melts that show a remarkable Arrhenius behavior over a large temperature domain [10]. Similarly to our sample, these strong melts are generally silica-rich and therefore strongly polymerized. However, viscosity is mostly controlled by Si–O bond relaxation time, which makes an important difference with the electrical conductivity of our melt being rate-controlled by Na migration. For example, the activation energy for the electrical conductivity of our sample is 70–61 kJ/mol, whereas for a sample with a similar composition, the activation energy for viscosity is ~450 kJ/mol [31]. Moreover, no change in the temperature dependence of electrical conductivity is observed as the sample crosses the melt–glass transition whereas viscosity of rhyolites does show a kink in an Arrhenius plot around T_g. This clearly illustrates that alkali diffusion is not related to viscosity and therefore does not obey the Eyring equation as suggested in [11]. Sodium must move without involving the breaking of Si–O bonds. Interpreting more in detail the transport mechanisms should be feasible by combination of the Nernst–Einstein equation and the frequency dependence of electrical conductivity [13,31]. Unfortunately the high-frequency signal was not accessible, which limits the understanding of microscopic transport mechanisms. Nevertheless, a remarkable feature revealed by the use of the Nernst–Einstein equation is that all Na ions in the melt act as charge carriers. The number of charge carriers is therefore not thought to be thermally activated, at least in the temperature range of this study. The effect of water on electrical conductivity reveals therefore an effect on Na mobility and not on the number of Na available for charge transport. In addition, a Haven ratio equal to 1 tells us that Na ions move independently of each other by an interstitial mechanism [13,32]. Addition of water enhances this interstitial migration probably by creating more interstitial sites and therefore facilitating the mobility of Na. Pressure, which decreases the electrical conductivity, must have an opposite effect on these interstitial sites. An increase in pressure reduces the porosity of the melt and must consequently reduce the possibility of interstitial migrations. The value of activation volume extracted (20 cm^3/mol) indicates a strong effect of pressure at least in the crustal range, which could be related to a relatively high compressibility of these silica-rich melt.

5.3. Charge carriers in magma and interpretation of magnetotelluric data

Fig. 9 shows the temperature dependence of electrical conductivity for several molten silicates collected from this study and the literature [13,16,33]. The activation energies are similar (~70 kJ/mol) for the dry sodium silicate, the dry Na-rich andesite and the dry rhyolite melt, which strongly supports the idea that Na mobility controls the electrical properties of these relatively Na-rich molten silicates [29]. For the hydrous obsidian, its low activation energy (64–61 kJ/mol) reflects also a control by Na mobility although it contains >10% H_2O mol. The activation energy for the conductivity of Na-bearing basalt is slightly higher (120 kJ/mol) but cannot be explained by the mobility of divalent cation having an activation energy around 250 kJ/mol, which is consistent with the conductivity of Na-free basaltic melts (Fig. 9). Electronic conductivity is prob-

ably not significant in the high-temperature region as suggested by extrapolation from low-temperature measurements [25,26,34] (see Fig. 9) and Waff and Weill [35], showing that changes in the ferric–ferrous ratio of basaltic melts do not affect their electrical conductivity. It seems therefore likely that Na controls also the electrical conductivity of natural basalts. The difference in activation energy between the rhyolitic–andesitic and the basaltic compositions is consistent with the fact that the activation energy for Na mobility is a function of Na content in melts [36]. Henderson et al. [22] have also shown how the activation energy for Na tracer diffusion greatly increases with decreasing Na content, reaching a value of 150 kJ/mol for Na-poor tholeiitic basalts. We therefore anticipate that both Na content and mobility would be responsible for the conductivity of basaltic to Na-rich rhyolitic melts, which could greatly simplify the interpretation of resistivity anomalies attributed to the molten region in the crust and in the mantle. In particular, Na, being an incompatible element, is preferentially incorporated in the liquid as magma crystallizes. A magma under differentiation becomes Na-richer and is therefore likely to show a particular electrical signature that could be elucidated from the marriage of laboratory and high-resolution geomagnetic measurements.

Hoffmann-Rothe et al. [6] revealed the presence of a conductive zone below Java, a volcanic area, which is probably attributable to a magma chamber at 6 km depth ($\sim$200 MPa). They determined a resistivity of 2 for this magma, which cannot reasonably reflect the presence of basaltic lava since it would correspond to a temperature higher than 1250°C. Considering the results of this study at 200 MPa, a resistivity of 2 would correspond to a dry rhyolite at 950°C, or a 1 wt% H_2O melt at 875°C, or a 3 wt% H_2O melt at 830°C or by extrapolation of Eq. 5, a 6 wt% water-bearing melt at 760°C. All these temperature–water content estimations are extremely realistic and consistent with what we know from phase equilibria in water-bearing magma [37]. Analyses of eruption products of Merapi volcano, located just above the identified magma chamber [6], reveal that most of the lavas have an andesitic bulk composition with a rhyolitic matrix [38] (3.5 wt% Na_2O). The Na content of the matrix is slightly lower than in the obsidian melt of this study and should therefore be slightly more resistive for a given temperature. This study clarifies the mechanisms of conduction in hydrous magma, but more has to be known about the combined effects of water and Na content on the electrical conductivity of melts. Furthermore, the crystal content of magma should affect slightly its electrical conductivity and must therefore be understood.

Multicomponent thermodynamic models such as MELTS tell us that parameters controlling the conductivity of a magma such as temperature, water, sodium and crystal contents are not independent parameters and, furthermore, they can be estimated. Combining phase equilibria models [37] of magmas upon differentiation and their electrical conductivity seems, therefore, to be a promising approach allowing the elucidation of maturity and water content of magmas stored within the Earth with some vital aspects concerning the estimation and anticipation of volcanic hazards.

6. Conclusion and perspectives

This paper describes a setup to perform high-P–high-T laboratory measurements of electrical conductivity of hydrous and dry obsidians. We show that the effect of pressure and temperature can be elucidated and rationalized using an Arrhenius law that reproduces measured electrical conductivity in the glass and the melt region. Therefore, for hydrous and dry obsidian, a change in the mechanisms of conduction across T_g is excluded. The conductivity of dry and hydrous rhyolites is shown to be exclusively controlled by sodium mobility and concentration. The positive effect of water on electrical conductivity is interpreted as the effect of water on sodium mobility.

Compilation of literature data on both electrical conductivity and tracer diffusion in natural and synthetic melts indicates that Na could be responsible for the electrical behavior of most terrestrial magmas, making the conductivity of mag-

mas stored in the Earth a potential probe of their maturity and differentiation degree.

Acknowledgements

The experimental work and the writing has benefited from the precious help of B. Schmidt, J. Mecklenburg and F. Bromiley. B. Poe is also acknowledged for the numerous and helpful discussions we had at the BGI before this work was initiated. E. Bailey, who pioneered, and instructed F.G., the use of the IHPV at the BGI, is warmly thanked. The reviews of J.D. Price and D. Dobson and the editorial work of B. Wood are acknowledged. This work was financed by the visitor program of the BGI.*[BW]*

References

[1] A.G. Jones, Imaging the continental upper mantle using electromagnetic methods, Lithos 48 (1999) 57–80.
[2] J. Pous, P. Queralt, J. Ledo, E. Roca, A high electrical conductive zone at lower crustal depth beneath the Betic Chain (Spain), Earth Planet. Sci. Lett. 167 (1999) 35–45.
[3] G.M. Partzsch, F.R. Schilling, J. Arndt, The influence of partial melting on the electrical behaviour of crustal rocks: laboratory examinations, model calculations and geological interpretations, Tectonophysics 317 (2000) 189–203.
[4] P.W.J. Glover, J. Pous, P. Queralt, J.A. Munoz, L. Montserrat, M.J. Hole, Integrated two-dimensional lithospheric conductivity modeling in the Pyrenees using field-scale and laboratory measurements, Earth Planet. Sci. Lett. 178 (2000) 59–72.
[5] Y. Xu, T.J. Shankland, B.T. Poe, Laboratory-based electrical conductivity in the Earth's mantle, J. Geophys. Res. B 105 (2000) 27865–27875.
[6] A. Hoffmann-Rothe, O. Ritter, V. Haak, Magnetotelluric and geomagnetic modeling reveals zones of very high electrical conductivity in the upper crust of Central Java, Phys. Earth Planet. Inter. 124 (2001) 131–151.
[7] J.J. Roberts, J.A Tyburczy, Partial-melt electrical conductivity: Influence of melt composition, J. Geophys. Res. B 104 (1999) 7055–7065.
[8] P.W.J. Glover, M.J. Hole, J. Pous, A modified Archie's law for two-conducting phases, Earth Planet. Sci. Lett. 180 (2000) 369–383.
[9] M.C. Johnson, A.T. Anderson, M.J. Rutherford, Pre-eruptive volatile contents of magmas, in: M.R. Carroll, J.R. Holloway (Eds.), Mineral. Soc. Am. Rev. Mineral. Volatiles Magmas 30 (1994) 281–323.
[10] A. Pfeiffer, Viscosities and electrical conductivities of oxidic glass-forming melts, Solid State Ionics 105 (1998) 277–287.
[11] J.E. Mungall, Empirical models relating viscosity and tracer diffusion in magmatic silicate melts, Geochim. Cosmochim. Acta 66 (2002) 125–143.
[12] S. Chakraborty, Diffusion in silicate melts, Mineral. Soc. Am. Rev. Mineral. 32 (1995) 411–504.
[13] I. Heinemann, G.H. Frischat, The sodium transport mechanism in $Na_2O.2SiO_2$ glass determined by the Chemla experiments, Phys. Chem. Glasses 34 (1992) 255–260.
[14] F. Gaillard, B. Schmidt, S. Mackwell, C. McCammon, Rate of hydrogen-iron redox exchange in silicate melts and glasses, Geochim. Cosmochim. Acta 67 (2003) 2427–2441.
[15] B.C. Schmidt, B. Scaillet, F.M. Holtz, Accurate control of fH_2 in cold-seal pressure vessels with the Shaw membrane technique, Eur. J. Mineral. 7 (1995) 893–903.
[16] J. Tyburczy, H.S. Waff, Electrical conductivity of molten basalt and andesite to 25 kilobars pressure: Geophysical significance and implications for the charge transport and melt structure, J. Geophys. Res. 88 (1983) 2413–2430.
[17] R.A. Lange, I.S.E. Carmichael, Thermodynamic properties of silicate liquids with emphasis on densitythermal expansion and compressibility, Rev. Mineral. 24 (1990) 25–64.
[18] E.B. Watson, Diffusion in volatile-bearing magmas, Mineral. Soc. Am. Rev. Miner. Volatiles Magmas 30 (1994) 371–411.
[19] J.R. Macdonald, Impedance Spectroscopy, Emphasizing Solid Materials and Systems, Wiley, New York, 1987, 346 pp.
[20] J.S. Hubner, R.G. Dillenburg, Impedance spectra of hot, dry silicate minerals and rocks: Qualitative interpretation of spectra, Am. Mineral. 80 (1995) 46–64.
[21] A. Jambon, Tracer diffusion in granitic melts: Experimental results fro Na, K, Rb, Cs, Ca, Sr, Ba, Ce, Eu to 1300°C and a model of calculation, J. Geophys. Res. 87 (1982) 797–810.
[22] P. Henderson, J. Nolan, G.C. Cunningham, R.K. Lowry, Structural controls and mechanisms of diffusion in natural silicate melts, Contrib. Min. Pet. 89 (1985) 263–272.
[23] Y. Zhang, E.M. Stolper, G.J. Wasserburg, Diffusion of water in rhyolitic glasses, Geochim. Cosmochim. Acta 55 (1991) 441–456.
[24] H. Behrens, R. Kappes, P. Heitjans, Proton conduction in glass- an impedance and infrared spectroscopic study on hydrous $BaSi_2O_5$ glass, J. Non-Cryst. Solids 306 (2002) 271–281.
[25] R.J. Barczyinski, L. Murawski, Mixed electronic-ionic conductivity in transition metal oxide glasses containing alkaline ions, J. Non-Cryst. Solids 307 (2002) 175–180.
[26] J.R. Jurado-Egea, A.E. Owen, A.K. Bandyopadhyay, Electronic conduction in basalt glass and glass-ceramics-correlation with magnetite crystallization, J. Mater. Sci. 22 (1987) 3602–3606.
[27] J.T. Blender, C.A. Edmondson, J.J. Fontanella, M.F.

Shlesinger, M.C. Wintersgill, Electrical conductivity in glass-forming solid electrolytes: theory and experiments, Solid State Ionics 154-155 (2002) 337–342.
[28] E.B. Watson, Diffusion in magmas at depth in the Earth: The effect of pressure and dissolved H_2O, Earth Planet. Sci. Lett. 52 (1981) 291–301.
[29] E.B. Lebedev, N.I. Khiratov, Dependence of the beginning of melting of granite and the electrical conductivity of its melt on high vapour pressure, Geochem. Int. 1 (1964) 193–197.
[30] J. Shatherley, S.I. Smedley, The electrical conductivity of some hydrous and anhydrous molten silicates as a function of temperature and pressure, Geochim. Cosmochim. Acta 49 (1986) 769–777.
[31] K.U. Hess, D.B. Dingwell, C. Gennaro, V. Mincione, Viscosity-temperature behaviour of dry melts in the Qz-Ab-Or system, Chem. Geol. 174 (2001) 133–142.
[32] B. Roling, What do electrical conductivity and electrical modulus spectra tell us about the mechanisms of ion transport processes in melts, glasses and crystals?, J. Non-Cryst. Solids 244 (1999) 34–43.
[33] G. Gruener, D. DeSousaMeneses, P. Odier, Influence of the network on conductivity in ternary CaO-Al2O3-SiO_2 glasses and melts, J. Non-Cryst. Solids 281 (2001) 117–124.
[34] A. Mogus-Milankovic, B. Santic, D.E. Day, C.S. Ray, Electrical conductivity in mixed-alkali iron phosphate glasses, J. Non-Cryst. Solids 283 (2001) 119–128.
[35] H.S. Waff, D.F. Weill, Electrical conductivity of magmatic liquids: effects of temperature, oxygen fugacity, and composition, Earth Planet. Res. Lett. 28 (1975) 254–260.
[36] H. Behrens, Na and Ca tracer diffusion in plagioclase glasses and supercooled melts, Chem. Geol. 96 (1992) 267–275.
[37] M.S. Ghiorso, R.O. Sack, Chemical mass transfers in magmatic processes: IV. A revised and internally consistent thermodynamic model for the interpolation and extrapolation of liquid-solid equilibria in magmatic systems at elevated temperatures and pressures, Contrib. Mineral. Petrol. 90 (1995) 197–212.
[38] J.E. Hammer, K.V. Cashman, B. Voight, Magmatic processes revealed by textural and compositional trends in Merapi dome lavas, J. Volcan. Geotherm. Res. 100 (2000) 165–192.
[39] C.T. Moynihan, Description and analysis of electrical relaxation data for ionically conducting glasses and melts, Solid State Ionics 105 (1998) 175–183.